PAPER

Check for updates

Phosphorylated cellulose paper as highly efficient adsorbent for cadmium heavy metal ion removal in aqueous solutions

El-Houssaine Ablouh, [ID] * Zineb Kassab, [ID] Fatima-zahra Semlali Aouragh Hassani, Mounir El Achaby [ID] and Houssine Sehaqui*

In search for more effective and eco-friendly adsorbent materials, this study comprehensively investigated Cd^{2+} adsorption onto phosphorylated cellulose paper (PCP). For this, cellulose microfibers (CMF) was extracted from Alfa fibers and phosphorylated using the solid-state phosphorylation approach. Then, the prepared PCP samples were characterized by SEM, EDX, XRD, FTIR, TGA, conductometric titration and zeta potential measurement. The adsorption of cadmium ions, the effect of time, pH and Cd^{2+} initial concentration were systematically studied in batch experiments. Based on the results, the highest adsorption capacity achieved was 479 mg of Cd^{2+} per g of PCP, which was remarkable compared to other modified cellulose capacities cited in the literature. Furthermore, the Cd^{2+} removal mechanism was investigated based on characterization results before and after adsorption and also based on the kinetics results. It was concluded that cation exchange and electrostatic attraction between phosphorylated cellulose and the cadmium ion mainly dominated the adsorption process. These findings highlighted that the phosphorylated cellulose paper has a broad application prospect in removal of divalent metal from aquatic solution.

1. Introduction

Cadmium is a toxic heavy metal that can easily accumulate in fish and plants, and subsequently enter into the human body through the food chain.[1] Its difficult degradation has been an important issue to address since it is hazardous not only to human health but also to ecological systems.[2,3] To remediate the negative effects of this heavy metal, a great importance has been placed on the development of highly efficient technology to remove it from aquatic environments. Hence, various treatments have been used to remove Cd^{2+} from contaminated waters, including membrane filtration,[4] chemical electrodeposition,[5] precipitation,[6] ion exchange and adsorption.[7,8]

Adsorption, which has gained a great deal of interest, is preferred because of its easy operation, high efficiency, fast pollutant removal rate, eco-friendly nature, low cost, and reversibility.[9–14] The commonly reported adsorbents materials are activated carbon,[15,16] zeolite,[17,18] clay,[19] apatite.[20] Despite materials' extensive use and good adsorption performance, the quest for cheap, environmentally benign, and excellent adsorbents is still ongoing. Consequently, cellulosic materials have surfaced as a potential candidate offering great application prospects in water treatment due to its numerous advantages,

such as low-cost, renewability, biodegradability and easy functionalization ability.[21–24] In its native state, cellulose has a small specific surface area and uncharged structure, and this is inconveniently limiting its adsorption efficiency.[25,26] Therefore, studies have been widely focused on improving the chemical and adsorption properties of native cellulose *via* the grafting of active functional groups on its backbone, thus allowing the immobilization of heavy metals ions. Most cellulose-based adsorbents reported in the literature focused on the grafting of amino and carboxyl groups. For instance, Li *et al.* investigated the Cd^{2+} adsorption property of carboxymethyl cellulose (CMC) bridged chlorapatite and showed that these materials can effectively remove Cd^{2+} with a maximum sorption capacity of 150.2 mg g^{-1}.[27,28] In addition, Quan *et al.* synthesized multifunctional-group modified cellulose adsorbent for cadmium removal in water, and the maximum adsorption capacity registered was 277 mg g^{-1}.[1] Surprisingly, little attention has been devoted to the use of phosphorylated cellulose as an adsorbent of cadmium ion despite the excellent metal-binding, ion exchange and adsorption features of the phosphate groups. Indeed, phosphate groups introduced to cellulosic chains can significantly enhance the adsorption capacity of metal ions and other pollutants due to their outstanding chelating property.[29,30] Nevertheless, this concept has not been demonstrated for enhanced removal of Cd^{2+} from polluted water.

Materials Science, Energy and Nanoengineering Department (MSN), Mohammed VI Polytechnic University (UM6P), Lot 660 – Hay Moulay Rachid, Benguerir, 43150, Morocco. E-mail: elhoussaine.ablouh@um6p.ma; houssine.sehaqui@um6p.ma

In the present study, phosphorylated cellulose extracted from Alfa fibers was prepared as a promising material for Cd^{2+} adsorption. Several characterization techniques were used to explore the physical and chemical properties of phosphorylated cellulose paper. The adsorption performance is evaluated by the removal of cadmium ions from aqueous solution. The results and the comparison with the literature indicate that the present green sorbent is among the most promising technologies for cadmium remediation from contaminated water.

2. Experimental section

2.1 Reagents

Cadmium nitrate tetrahydrate 98%, dibasic ammonium phosphate ($(NH_4)_2HPO_4$; 98%) and urea (99%) were purchased from Sigma Aldrich and used as received without prior purification.

2.2 Cellulose extraction from Alfa grass

Alfa, also called esparto grass or *Stipa tenacissima* was collected from the oriental region of eastern Morocco, and used for cellulose extraction according to standard alkaline and bleaching treatments. Details on the extraction process and on the properties of extracted cellulose can be found in previous publications.[31] In brief, 10–20 mm small fibers were cut from the original Alfa grass. These fibers were first treated with 60 °C hot distilled water for one hour. Subsequently, a NaOH treatment with a 4 wt% solution was done at 80 °C for 2 h under stirring and repeated 3 times ensuring the alkali-treatment of cellulose. Finally, a bleaching treatment was repeated three times resulting in white-colored cellulose fibers. The bleaching was performed using a solution made up of equal parts (v/v) of aqueous sodium chlorite at 1.7 wt% and acetate buffer. This latter was prepared by diluting 27 g NaOH and 75 mL glacial acetic acid to 1 L of distilled water. In all these treatments, the ratio of the fibers to liquor was 1/20 (g/mL).

2.3 Phosphorylated cellulose paper preparation

A solution containing 5.1 g dibasic ammonium phosphate and 12 g of urea dissolved in 25 mL distilled water was first prepared. Then 10 g of the extracted Alfa cellulose was soaked in that solution, and the mixture was dried overnight at 60 °C. The phosphorylation reaction was triggered by heating the whole to a temperature of 150 °C for 60 min. Subsequently, unreacted species were thoroughly washed from the modified cellulosic fibers by distilled water, and the resulting phosphorylated fibers were freeze-dried. Thereafter, the phosphorylated fibers were swollen in 1 M sodium hydroxide solution, washed again until the pH was neutral, and mechanically treated at a concentration of 1 wt% in a probe sonicator for 20 minutes. Finally, the well-dispersed phosphorylated cellulose suspension (300 mg dry weight) were casted in a polystyrene Petri-dish (80 mm in diameter), and the water was evaporated giving a phosphorylated cellulose paper. This latter was thermally crosslinked (hornified) at 150 °C for 1 hour to confer it water stability.

2.4 Characterizations

2.4.1 Attenuated total reflection Fourier transform infrared spectroscopy analysis (ATR-FTIR). The functional groups of the native and phosphorylated fibers were analyzed using Fourier Transform Infrared Spectroscopy (FTIR, PerkinElmer) operated from 4000 to 400 cm^{-1} at 4 cm^{-1} step by attenuated total reflection (ATR).

2.4.2 X-ray diffraction analysis (XRD). XRD analysis was done at room temperature using a Bruker diffractometer (copper anode [$K_\alpha = 1.5418$ Å]). The diffractograms were recorded in the range $2\theta = 5$–$40°$ with a step size of $0.02°$.

2.4.3 Scanning electron microscopy with energy-dispersive X-ray analysis (SEM-EDX). Surface morphology of cellulosic fibers before and after phosphorylation process was done with TESCAN-VEGA3 scanning electron microscopy at an accelerating voltage of 10 kV. Energy dispersive X-ray (EDAX) analyzer was employed to depict the specific elemental composition and distribution in phosphorylated cellulose paper (PCP) surface before and after adsorption. All samples were attached on SEM specimen holders with double-sided carbon tape and coated with gold by using high vacuum sputter coater.

2.4.4 Thermogravimetric analysis (TGA). The thermal properties of phosphorylated cellulose paper were studied by thermogravimetry (TA instrument). The sample thermal stability was evaluated under nitrogen flow (20 mL min^{-1}), from 25 to 700 °C with a heating rate of 10 °C min^{-1} wherein approximately 8 mg of the sample was placed in open platinum pans.

2.4.5 Total charge content determination. A conductometric titration was used to determine the total charge content of the phosphorylated fibers. In brief, 5 mL of NaCl at 0.01 M was added to 0.3 g of the phosphorylated fibers suspended in 85 mL of water. Then, hydrochloric acid was added to the mixture to set the pH to 2.5–3. Finally, the mixture was titrated by several additions of NaOH solution (100 μL at 0.05 M) while monitoring the electrical conductivity and pH of the fiber suspension. This was continued until the pH of the suspension reached 11. The negative charges content was determined from the middle line of the curve showing electrical conductivity *versus* volume of NaOH added.

2.4.6 Zeta-potential measurement. Zeta potential measurements as a function of pH were carried out using a Malvern Zeta sizer Nano ZS instrument wherein a capillary cell of zeta cells (Product No. DTS1070, Malvern Instruments) was used. Phosphorylated cellulose fiber suspensions were diluted and sonicated for 15 min before being analyzed. Then, NaCl was added to each sample so that a final concentration of 1 mM is reached. After decanting for 20 min, the pH value of the paste was recorded and the supernatant was collected for zeta potential measurements.

2.5 Batch adsorption experiments

Adsorption experiments were performed in batch system with distilled water being used to prepare the synthetic solutions. A stock solution of Cd^{2+} at 1000 mg L^{-1} was prepared by dissolving an appropriate amount of the analytical grade reagent
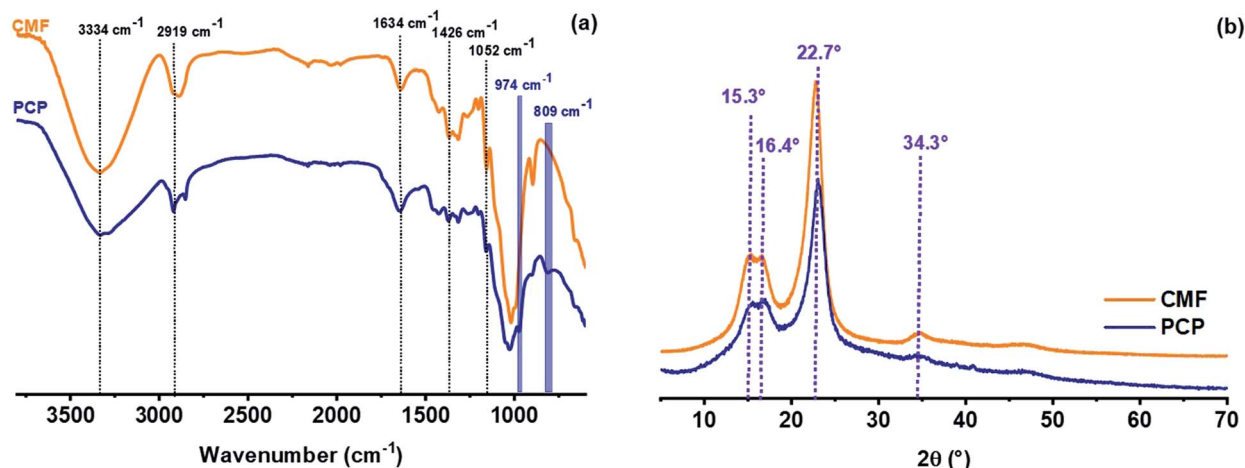
Fig. 1 FTIR spectra (a) and XRD patterns (b) of cellulose microfibers (CMF) and phosphorylated cellulose paper (PCP).

$(Cd(NO_3)_2)$ in distilled water. Cd^{2+} solutions of lower concentrations were obtained by diluting the stock solution with distilled water just before the adsorption experiments. In order to adjust the pH of the medium, 0.1 M of NaOH or 0.1 M of HCl were used. All cadmium adsorption batch experiments were carried out at room temperature (25 ± 3 °C) in a 120 mL beaker in which 20 mg of dried PCP was immersed together with 100 mL of Cd^{2+} solution. The stirring speed was maintained at 150 rpm. The kinetic studies were performed at different initial concentrations (20–300 mg L^{-1}) at pH = 6. The Cd^{2+} concentration was measured using Cadmium Ion-Selective Electrode (C-ISE, Thermoscientific, Orion 9648BNWP). The adsorption capacities at any time t (q_t), at equilibrium (q_e) and the amount of Cd^{2+} adsorbed onto PCP ($R\%$) were calculated with the following equations:

$$q_t (\text{mg/g}) = \frac{C_0 - C_t}{W} \cdot V \quad (1)$$

$$q_e \left(\frac{\text{mg}}{\text{g}}\right) = \frac{C_0 - C_e}{W} \cdot V \quad (2)$$

$$R(\%) = \frac{C_0 - C_t}{C_0} \cdot 100 \quad (3)$$

where C_0 (mg L^{-1}) is the initial concentration of Cd^{2+}, C_t (mg L^{-1}) is the concentration of Cd^{2+} at time t, w (g) is the dry weight of the PCP adsorbent, and V (L) is the volume of the aqueous solution.

3. Results and discussions

3.1 Structural, physical and surface properties of phosphorylated cellulose paper

Phosphorylated cellulose was produced from cellulose microfibers extracted from Alfa grass. The success of phosphorylation reaction was first confirmed by means of FT-IR spectroscopy, thermogravimetric analysis and conductometric titration. From the FTIR spectra (Fig. 1a), the cellulose microfibers (CMF) showed characteristic bands at 3334, 2895 and 1052 cm^{-1} corresponding respectively to stretching vibrations of O–H, C–H and C–O–C of the glucosidic units.[31] Other absorption bands around 1649 cm^{-1} and 1426 cm^{-1} were assigned to the O–H bending of adsorbed water and C–H bending vibrations, respectively.[31,32] The phosphorylation of cellulose microfibers was supported by the appearance of several new bands characteristic of phosphate groups grafted in cellulosic chains. The most intense of these bands are located at 809 cm^{-1} and are
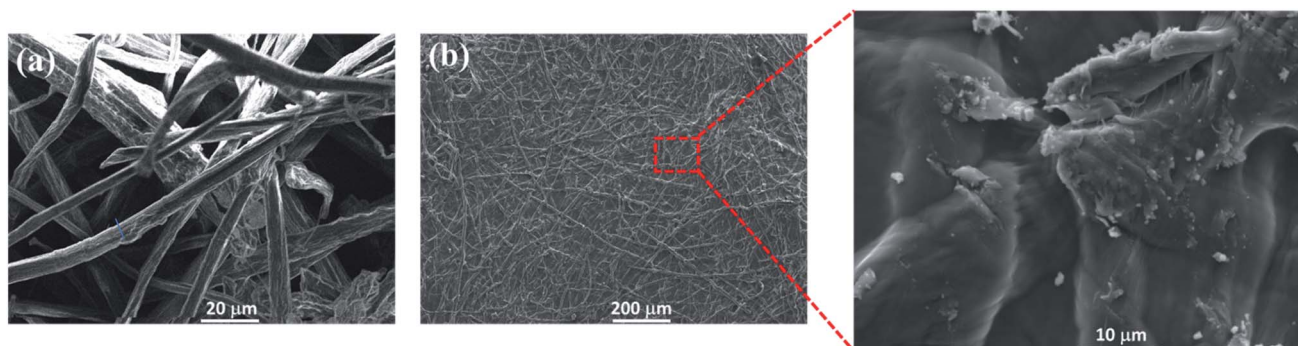

Fig. 2 SEM images of cellulose microfibers (a) and phosphorylated cellulose paper (b).
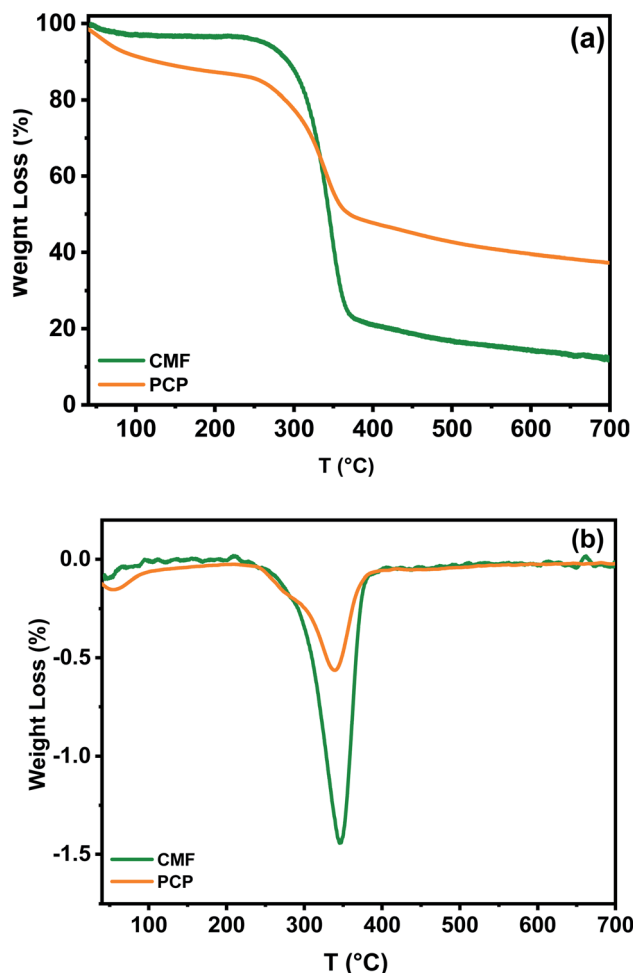
Fig. 3 (a) TGA and (b) DTG curves for cellulose microfibers (CMF) and phosphorylated cellulose paper (PCP).

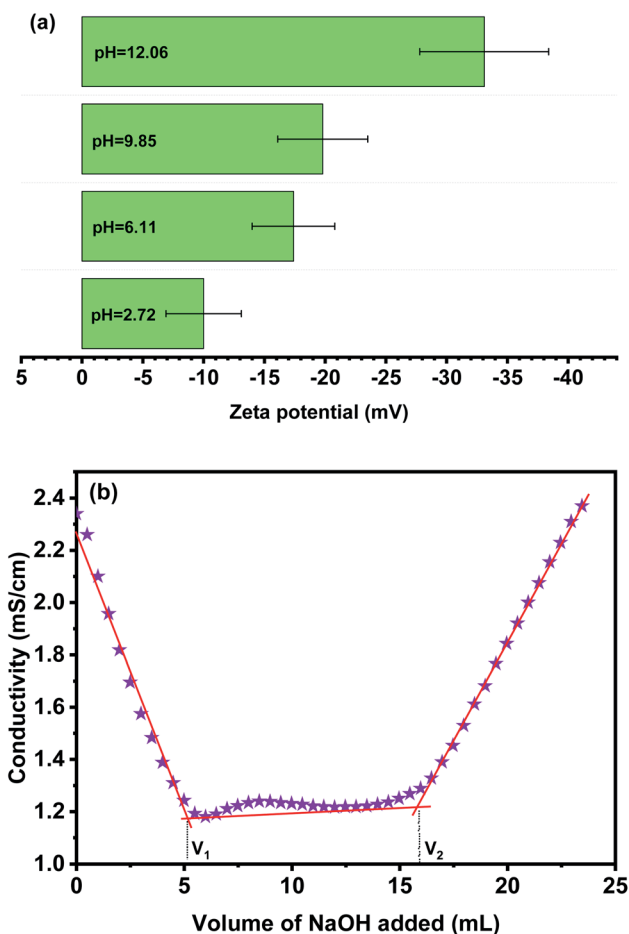Fig. 4 Zeta potential measurements as a function of pH (a) and conductivity titration curve (b) of phosphorylated cellulose.

assigned to vibration of P–O–C aliphatic bond.[33] In addition, the IR spectra exhibited new band at 974 cm^{-1} corresponding to bending vibration of P–OH,[33,34] which confirms that the phosphate groups were successfully introduced into the cellulosic fibers.

Cellulose commonly consists of both crystalline and amorphous regions.[35] Such crystalline structure is due to hydrogen bonding interactions and van der Waals forces between adjacent cellulosic monomers.[36] Identification of cellulosic materials by evaluating their crystallinity after different chemical treatment steps was done using X-ray diffraction. Fig. 1b presents the XRD of extracted cellulose microfibers (CMF) and PCP. The CMF exhibited four main reflection peaks at $2\theta = 15.3°$, $16.4°$, $22.7°$ and $34.4°$, which are attributed to the crystalline form of native cellulose (cellulose I).[37] Similarly, the same peaks were obtained for PCP indicating that the phosphorylation of cellulose occurs without alteration of the crystalline form of cellulose.

Scanning electron microscopy was carried out to get more insight on the morphology of phosphorylated cellulose paper. SEM image of the cellulose microfibers extracted from Alfa fibers show an average fiber diameter of 7.6 ± 1.5 μm (Fig. 2a).

The PCP sample exhibits typical paper structure wherein the fibers are randomly oriented in the plane direction.[38] Moreover, the fiber structure is maintained in the PCP sample (Fig. 2b), with fibrous structure strongly bonded to each other, as shown in the zoomed area of Fig. 2b. This might be attributed to the thermal treatment (hornification) of the PCP.

3.1.1 Thermal stability of phosphorylated cellulose paper. The thermal stability of cellulose microfibers and phosphorylated cellulose paper was investigated by thermogravimetric analysis. It can be seen in Fig. 3a that the CMF showed a two steps thermal degradation process under nitrogen gas flow, which are well explicated in the literature.[39] The first stage, occurring at lower temperatures range between 30 and 120 °C, is assigned to discharging of adsorbed hydrogen bond linked water, which is obvious because of cellulose fibers hydrophilicity. The intensive decomposition of cellulosic chains occurs in the second stage in the temperature range of 245–410 °C, and is due to the depolymerization of glycosyl units to volatile species by the cleavage of the main chain.[34] From the DTG curve, it can be seen that the cellulose microfibers show a main degradation peak temperature at around 350 °C. At temperatures above 400 °C, the decomposition (mass loss) is continued without any maximum rate observed (Fig. 3b). It should be

added that the residual char for cellulose microfibers is 14.2% at 700 °C.

Compared to CMF, the presence of phosphorus in the structure of PCP caused a considerable reduction in the cellulosic materials degradation towards char formation. This decrease is due to the catalyzed dehydration of cellulose by phosphoric acid, which was formed by the decomposition of phosphate groups at lower temperatures.[34] TGA and DTG curves of PCP also exhibit three clear steps and peaks of decomposition in the studied temperature range (Fig. 3a and b). The first peak detected between 50 and 92 °C, does not relate to a change of chemical structure of phosphorylated fibers during heating, but is associated to physically adsorbed water molecules. However, a comparison with the TGA curve of CMF indicate that the presence of phosphate in the PCP enhanced its susceptibility to water sorption, as indicated by Barud *et al.*[40] The second degradation phase of PCP, could be attributed to its pyrolysis,[41] which is headed by a smaller weight loss (5%) and appears as a shoulder at 254 °C. The third peak at 342 °C can be due to the depolymerization of the same units to thermally stable aromatic char, which forms the final residue at the end of the test.[42] Besides that, the final residual mass after the TGA analysis of

PCP was 40%. These results indicate that the presence of phosphorus increased the amount of charred residue produced, which is in agreement with literature reports.[43]

3.1.2 Surface charge and charge content of phosphorylated cellulose paper. Generally, the effectiveness of an adsorbent material is most prominently affected by their surface charge. For this reason, to understand the surface charge characteristics of PCP, the zeta potential was determined under different pH by a solid surface zeta potentiometer, as shown in Fig. 4. The determination of surface charge by zeta potential is not only to confirm the success of the phosphorylation process, but also is more sensitive to show surface changes from the introduced phosphates groups. Over the whole examined pH range, the PCP exhibit a negative charge due to the presence of phosphate groups. The obtained results indicate that with the increase of pH value, the zeta-potential increased in absolute value to -33.1 ± 7.3 at pH $= 12$, suggesting an improved electronegativity at higher pHs. In addition, the phosphorylated cellulose from Alfa was titrated by conductimetric method with NaOH in order to determine the total charge content of phosphate groups, which reached a maximum value of 3.3 mmol g^{-1} (Fig. 4b). This value
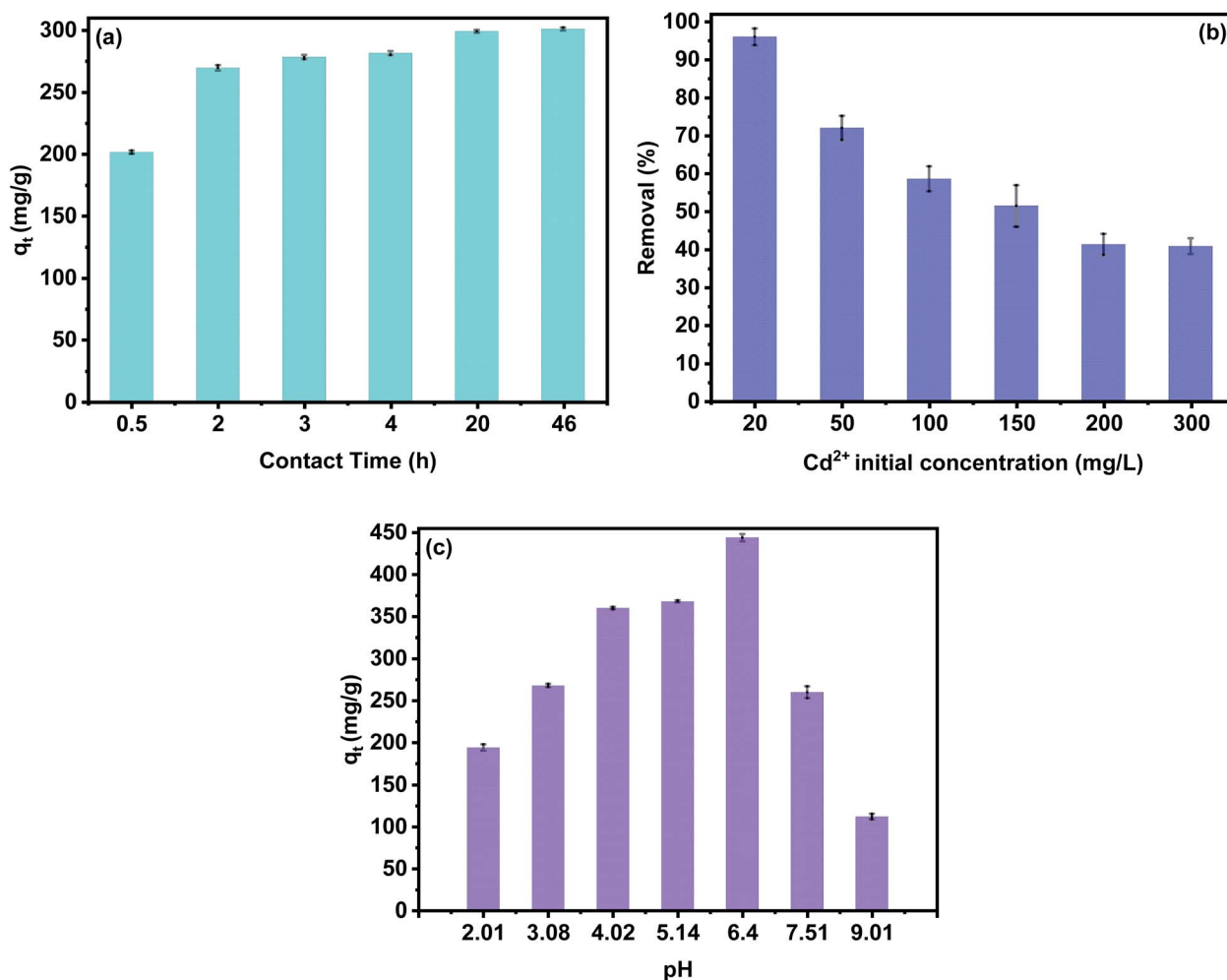

Fig. 5 Effect of Cd^{2+} contact time (a), initial concentration (b), pH value (c) on the Cd^{2+} adsorption.
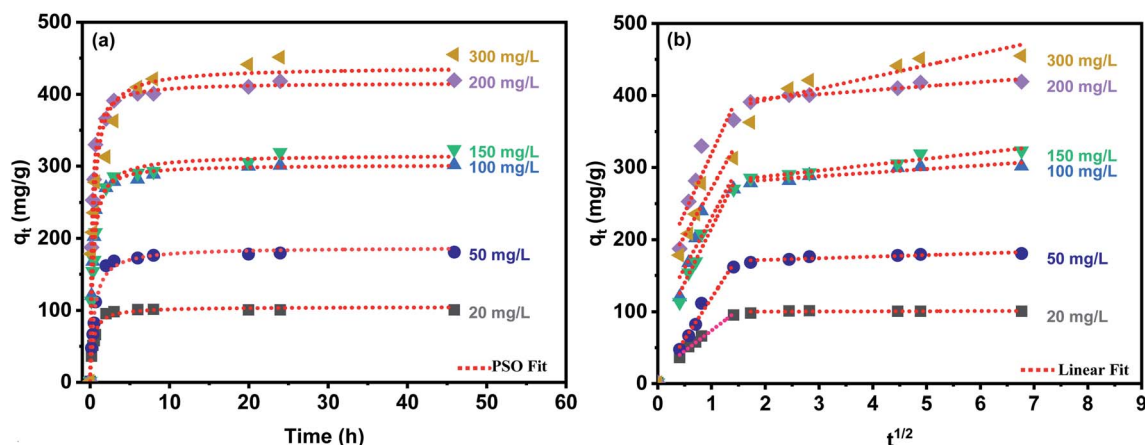
Fig. 6 Pseudo-second order model (a) and intra-particle diffusion model (b) of Cd^{2+} adsorption onto the PCP adsorbent.

Table 1 Parameters of kinetics models for the adsorption of Cd^{2+} on PCP adsorbent

		20 mg L^{-1}	50 mg L^{-1}	100 mg L^{-1}	150 mg L^{-1}	200 mg L^{-1}	300 mg L^{-1}
PFO	q_e (exp) (mg g^{-1})	100.267 ± 1.488	179.975 ± 2.863	301.250 ± 4.425	322.750 ± 9.851	419.250 ± 8.131	451.001 ± 15.556
	q_e (mg g^{-1})	98.971 ± 1.456	175.141 ± 2.021	249.745 ± 18.488	298.326 ± 6.911	350.431 ± 23.636	409.799 ± 17.289
	k_1	1.874 ± 0.119	1.408 ± 0.070	2.675 ± 0.237	1.926 ± 0.193	3.86 ± 0.651	1.900 ± 0.347
	Reduced Chi-sqr	14.08431	25.424	375.932	318.706	614.463	198.480
	R-square (COD)	0.988	0.994	0.603	0.971	0.646	0.907
	Adj. R-square	0.987	0.993	0.563	0.968	0.611	0.897
PSO	q_e	103.929 ± 1.532	186.478 ± 3.381	301.294 ± 3.050	315.192 ± 3.913	416.026 ± 3.126	437.681 ± 12.093
	k_2	0.027 ± 0.002	0.010 ± 0.001	0.013 ± 0.010	0.008 ± 0.007	0.011 ± 0.006	0.005 ± 0.001
	Reduced Chi-sqr	11.271	48.882	49.066	73.151	52.917	682.601
	R-square (COD)	0.990	0.988	0.994	0.993	0.996	0.968
	Adj, R-square	0.989	0.987	0.994	0.992	0.996	0.964

is within values registered for phosphorylated cellulose from various origins.[29]

3.2 Adsorption of cadmium performance study

3.2.1 Effect of variables on adsorption performance.
In order to determine the adsorption performance of the PCP, the effect of various factors such as: contact time, pH and Cd^{2+} initial concentration was studied. Fig. 5a shows the effect of contact time on the Cd^{2+} adsorption capacity. Results show that the removal efficiency of cadmium ions increased with the increase in adsorption time and the efficiency was slow at the end of the adsorption process due to the occupancy of the adsorption sites and pore spaces with cadmium ions. As given in Fig. 5a, most of the Cd^{2+} ions were removed from aqueous media between 1 hour and 4 hours, which allows us to select a higher contact time of 12 hours for further study. It must be noted that the effects of contact time on adsorption performance of PCP showed the same tendency for all Cd^{2+} initial concentrations. Therefore, we only focus on the 100 mg L^{-1} in the present discussion.

Initial metal ion concentration plays an important role in the adsorption of cadmium ions. The adsorption was investigated by varying C_0 from 20 to 300 mg L^{-1}. The results show that the removal efficiency of Cd^{2+} decreased from 96% to 40% with the increase of C_0 from 300 mg L^{-1} to 20 mg L^{-1}. This can be

explained by the number of adsorption sites limited by the adsorbent dose, so the removal percentage decreased with the increase of C_0. Generally, a high concentration of adsorbate leads to more occupied adsorption sites and quicker saturation.[1,9,11] On the other hand, the efficiency of the adsorption process depends on pH due to the protonation or deprotonation of phosphate groups, surface properties, and ionization ability of the cadmium. As can be seen in Fig. 5c, the Cd^{2+} uptake increased from 194 to 444 mg g^{-1} when the pH was increased from 2.01 to 6.40, respectively. This can be explained by the fact that free-form H^+ ions concentration increases with low pH in the solution, which lead to competition between the hydrogen

Table 2 Parameters of isotherm models for the adsorption of Cd^{2+} onto PCP adsorbent

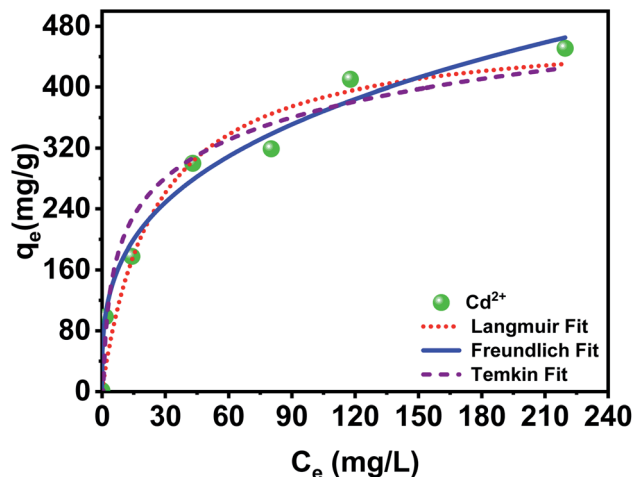| Isotherm	Parameters	
Langmuir	q_{max} (mg g^{-1})	479.920 ± 47.107
	K_L (L mg^{-1})	0.0394 ± 0.014
	Adj. R-square	0.991
Freundlich	K_F ((mg g^{-1}) (L mg^{-1})$^{1/n}$)	84.477 ± 11.602
	n	3.162 ± 0.295
	Adj. R-Square	0.984
Temkin	K_T (L g^{-1})	1.571 ± 0.821
	B	72.687 ± 8.732
	Adj. R-square	0.955

Fig. 7 Adsorption isotherms of PCP adsorbent for the removal of Cd^{2+}.

ions and Cd^{2+} cations, resulting in low removal efficiency. On the contrary, free-form hydrogen ions concentration decreases with the increase of pH, providing deprotonation of phosphates groups, which lead to high negative surface charges of the PCP adsorbent. Moreover, the sorption capacity decreases continually for initial pH values above 6.50. However, when the pH is further increased, Cd^{2+} cations may gradually convert to $Cd(OH)^+$, $Cd(OH)_2$, $Cd(OH)_3^-$ and $Cd(OH)_4^{2-}$, and the decrease in electrostatic attraction with the PCP adsorbent surface consequently results in unfavorable retention of Cd^{2+}.[44,45]

3.2.2 Kinetics study on adsorption performance. Kinetic studies are essential to evaluate the adsorption capacity of adsorbent materials and to estimate the adsorption mechanism. As discussed elsewhere in Section 3.2.1, the effect of contact time indicate that the PCP adsorbent has a strong affinity for the Cd^{2+} ions. Moreover, the adsorption kinetics can be controlled by the diffusion of mass, film and intra-particle.[44]

In this study the adsorption kinetics of PCP adsorbent was investigated using the Lagergren pseudo-first-order (eqn (4)), the pseudo-second-order (eqn (5)) and the intra-particle diffusion (eqn (6)) kinetic models.

$$q_t = q_e(1 - e^{-k_1 t}) \tag{4}$$

$$q_t = \frac{q_e^2 k_2 t}{1 + k_2 q_e t} \tag{5}$$

$$q_t = k_i t^{1/2} + C \tag{6}$$

where q_t and q_e are the amounts of Cd^{2+} uptake per mass (mg g^{-1}) of the PCP adsorbent at any time t and at equilibrium, respectively. k_1 (1/min), k_2 (g mg^{-1} min^{-1}) and k_i (mg g^{-1} min^{-1}) are the rate constants of the pseudo-first-order, pseudo-second-order, and intra-particle diffusion models, respectively.

Fig. 6a shows the best model fits the experimental kinetic data, and Table 1 gives the parameters of kinetics models. It can be seen that the experimental data are well described by the pseudo-second-order (PSO) model which well fitted the entire kinetic data with good correlation coefficient ($R^2 > 0.98$). Moreover, the values of q_e (mg g^{-1}) obtained from PSO agree entirely with the experimental q_e (exp) values (Table 1). Therefore, it is concluded that the PSO kinetic model and the process may be an exchange of electrons between adsorbent and adsorbate, which is in line with previous studies.[44,46] Rate-controlling steps for the PCP were evaluated by applying the intra-particle diffusion model. According to this model, if the plot of q_e versus $t^{1/2}$ gives a straight line, then the adsorption process is governed by intra-particle diffusion, and if the data reveal multi-linear plots, then two or more steps rule the adsorption process[11] shown in Fig. 6b, the intra-particle plot presents two distant linear plots and did not pass the origin, which indicates that the adsorption process is governed by more than one mechanism such as external mass transfer and intra-particle diffusion.
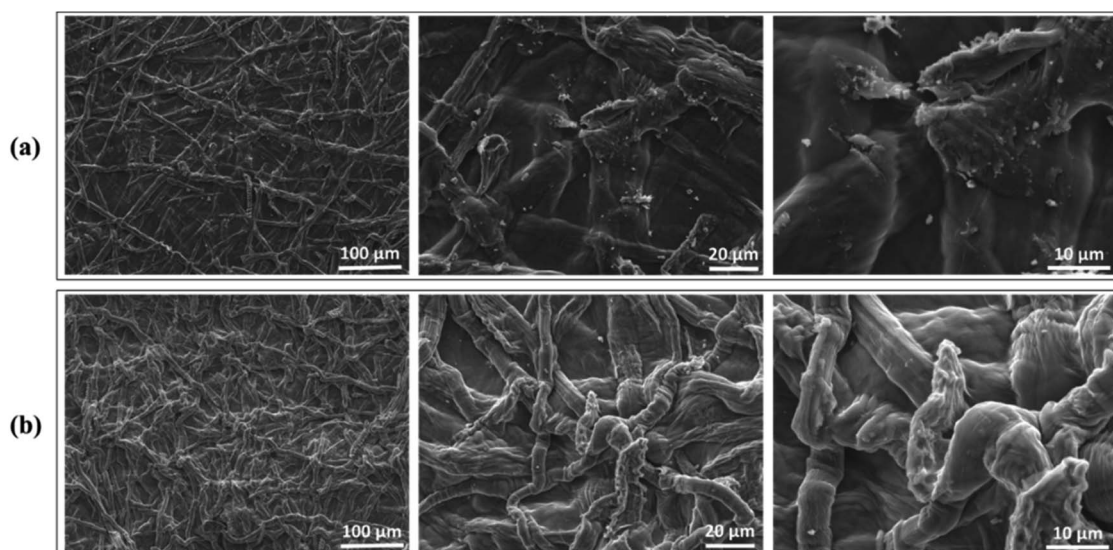

Fig. 8 SEM images a different magnification of PCP before (a) and after (b) Cd^{2+} loading.

3.2.3 Isotherms study and adsorption performance.

Isotherm models are frequently applied in batch experiments to determine the most suitable adsorption equilibrium behavior, and to evaluate the adsorbent performance under different experimental conditions. In this study, three isotherm models, namely Langmuir (eqn (7)), Freundlich (eqn (8)) and Temkin (eqn (9)) were fitted to the experimental data and the isotherm parameters obtained from these equations are presented in Table 2.

$$q_e = \frac{q_{max} K_L C_e}{1 + K_L C_e} \quad (7)$$

$$q_e = K_F C_e{}^n \quad (8)$$

$$q_e = B \ln K_T + B \ln C_e \quad (9)$$

where K_L (L mg^{-1}) represents the Langmuir affinity constant, C_e is the equilibrium concentration of Cd^{2+} in the solution phase (mg L^{-1}), q_e is the equilibrium uptake and q_{max} refers to the maximum Langmuir adsorption capacity (mg g^{-1}). K_F ((mg g^{-1}) (L mg^{-1})$^{1/n}$) and K_T (L mg^{-1}) are the Freundlich isotherm constant and Temkin isotherm constant, respectively.

In order to quantify the maximum adsorption capacity of PCP, adsorption experiments were performed with varying initial Cd^{2+} concentration. The results were fitted to the Langmuir, Freundlich and Temkin isotherm models. The comparison of the experimental values and the predicted amount with different isotherm models is given in Table 2. As expected, the adsorbed Cd^{2+} amount increases with the equilibrium concentration and eventually stabilizes at high C_e values. The typical maximum adsorption capacity reported for PCP is 479.920 ± 47.107 mg g^{-1}. Evidently, PCP provided much greater Cd^{2+} adsorption capacity than cellulose and other cellulose derivatives reported adsorbent materials. For example, Li et al.,[27] studied the adsorption of Cd^{2+} using carboxymethyl cellulose-bridged chlorapatite nanoparticles, and obtained a maximum adsorption capacity (q_{max}) of 150.13 mg g^{-1}. Ayouch et al.[45] reported a q_{max} of 126.58 mg L^{-1} using crosslinked carboxymethyl cellulose–hydroxyethyl cellulose hydrogel films. The high adsorption capacity attained is assigned to the surface charge density of the phosphorylated cellulose paper. Langmuir q_{max} value is close to the experimental data and is the best isotherm for forecasting the amount of Cd^{2+} adsorbed on the PCP adsorbent at equilibrium (Fig. 7). Therefore, the adsorption of Cd^{2+} occurs in ideal monolayer adsorption with a homogeneous surface, which could be explained by the fact that the adsorption of Cd^{2+} onto the PCP was encouraged by the negative phosphate groups formed on the surface that are highly reactive and can bind with cationic elements.

3.2.4 PCP adsorbent properties before and after Cd^{2+} loading: adsorption mechanism.

Generally, the adsorption capacity of adsorbent materials is affected by their surface properties such as porous structure, functional groups, chemical composition, and sorbent characteristics, which makes the removal mechanism very complex.[44] This study investigated the possible interaction of the phosphorylated cellulose with Cd^{2+}
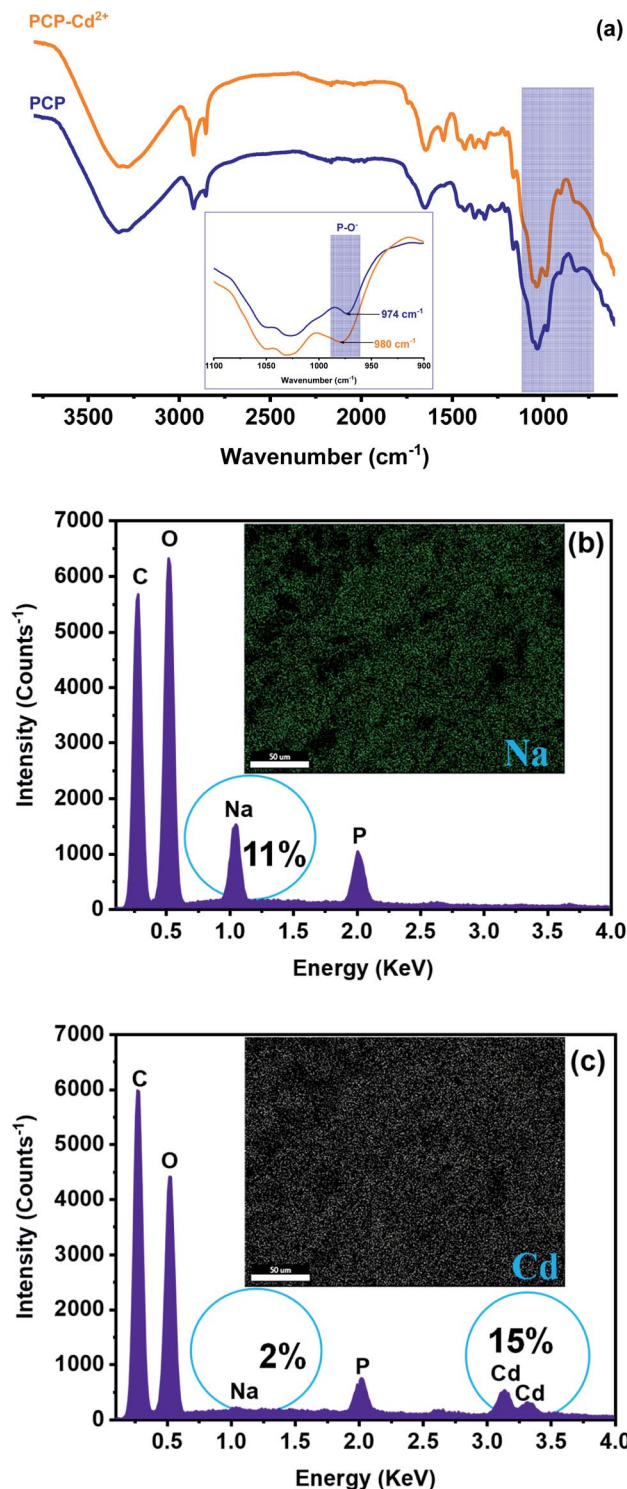

Fig. 9 FTIR analysis (a) and EDX spectra and P-elemental mapping of the PCP adsorbent surface before (b) and after (c) Cd^{2+} loading.

ion by exploring the PCP adsorbent surface before and after the adsorption process. The microstructure and morphology of PCP and PCP loaded Cd^{2+} surface were also examined, and the SEM photos are shown in Fig. 8. It can be observed that the surface morphology of PCP adsorbent and thus the microstructure of
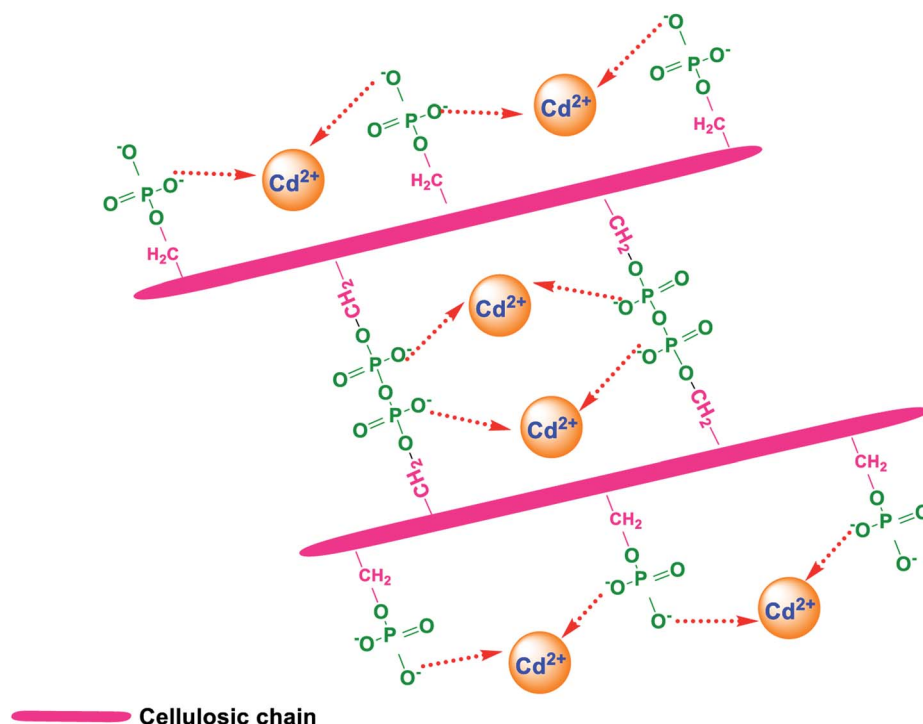
Fig. 10 Proposed Cd^{2+} adsorption mechanisms for PCP adsorbent.

fibers were affected. The PCP surface is more compact with evenly distributed fibers, while the fibers with adsorbed cadmium display a rougher and brighter surface.

The chemical composition of PCP before and after Cd^{2+} loading was also determined to further investigate the adsorption mechanism, and the result is displayed in Fig. 9. Generally, bivalent metals (M^{2+}) adsorption from aqueous system is carried out by complex chemical reactions and various mechanisms such as: electrostatic interaction, physical adsorption, ion exchange, complex formation, surface complexation, and precipitation.[13,27,46] To some extent, adsorption mechanism can be explained based on chemical composition results of adsorbent surface before and after adsorption. Moreover, it could be seen from elemental analysis (Fig. 9b and c) that the amount of sodium, which is present as a counter ion of deprotonated phosphate groups in the PCP adsorbent, was found to decrease from 11% to 2% after adsorption. Such reduction was counterbalanced by the increase in Cd content in the PCP,

suggesting that the adsorption mechanism was mainly the ion exchange between Cd^{2+} in aqueous solution and Na^+ on PCP adsorbent surface.

On the other hand, FTIR spectra shows a shift of P–O$^-$ stretching peak from 809 to a higher frequency region (817 cm^{-1}) of the infrared spectrum after Cd^{2+} adsorption (Fig. 9a). This shifting in wavenumber suggests that the oxygen atoms of phosphates groups (P–O$^-$) can be the attachment sites for cadmium ion.[9]

To sum up, based on structural, morphological, elemental analyses, the possible mechanisms of Cd^{2+} removal by PCP adsorbent are as follows: (1) ion-exchange between Na^+ on the adsorbent surface and Cd^{2+} ions in the aqueous solution, and (2) electrostatic attraction (Fig. 10).

Table 3 presents maximum adsorption capacity values of Cd^{2+} onto phosphorylated cellulose paper elaborated in this study and onto various cellulose-based adsorbents cited in the literature. Typical maximum adsorption capacities reported for

Table 3 Maximum adsorption capacity of different adsorbents–based cellulose used for the removal of Cd^{2+} from aqueous solution

Adsorbent based on cellulose	q_{max} (mg g^{-1})	References
Crosslinked carboxymethyl cellulose-hydroxyethyl cellulose hydrogel films	126.58	45
Cellulose	60.24	1
Multi-functional group modified cellulose	277.00	1
Cellulose-*graft*-polyacrylonitrile	12.09	47
Cellulose-*graft*-poly(acrylic acid)	18.66	47
Carboxymethyl cellulose-bridged chlorapatite nanoparticles	143.25	27
Carboxylated cellulose nanocrystals	256.30	48
Phosphorylated cellulose paper	479.92	This study

cadmium ions are between 18 and 500 mg g^{-1}. This comparison showed that the PCP has a higher adsorption capacity than any compared materials used under similar conditions. For instance, a carboxymethyl cellulose-bridged chlorapatite nanoparticles sorbent developed by Li *et al.* has about 3 times lower adsorption capacity, while crosslinked carboxymethyl cellulose/hydroxyethyl cellulose hydrogel films presented by Ayouch *et al.* have about 4 times lower adsorption capacity. The surface charge of adsorbent is the main factor that affect the removal efficiency of cationic ions; highly negatively charged surfaces enable more retention of cations. Phosphorylated cellulose paper show high adsorption capacity because of its high negative surface charge related to deprotonation of phosphate groups, which can interact easily with Cd^{2+} cation by electrostatic attraction, or by ion exchange between Na$^+$ and Cd^{2+} (Fig. 9).

4. Conclusion

This study reports an easy preparative route for functionalized cellulose with phosphate groups, effectively removing heavy cadmium metal from aqueous solution under optimized environmental conditions. The phosphorylated cellulose paper has a strong binding ability and exhibits good adsorption performance to Cd^{2+}, reaching the largest maximum Langmuir sorption capacity of 479.92 mg g^{-1}. pH is an important parameter influencing the adsorption capacity, giving a removal capacity lower than 194 mg g^{-1} when the solution initial pH is lower than 2, and more than 400 mg g^{-1} when the solution initial pH is between 5 and 6 pH units. Adsorption kinetic study revealed that most adsorption was achieved within the first three hours, and the pseudo-second-order model well fitted the kinetic data. Analyses of PCP adsorbent before and after adsorption, revealed that the mechanisms for removing cadmium ions included ion-exchange and electrostatic interaction. Overall, phosphorylated cellulose paper holds great promise to be used as an effective adsorbent material for removal of heavy metals from contaminated water.

Conflicts of interest

There are no conflicts to declare.

Acknowledgements

References

1 Q. Chen, J. Zheng, L. Wen, C. Yang and L. Zhang, *Chemosphere*, 2019, **224**, 509–518.

2 A. Satya, A. Harimawan, G. Sri Haryani, M. A. H. Johir, L. N. Nguyen, L. D. Nghiem, S. Vigneswaran, H. H. Ngo and T. Setiadi, *Environ. Technol. Innovat.*, 2021, **21**, 101194.

3 M. Abatal, M. T. Olguin, Y. Abdellaoui and A. El Bouari, *Environ. Prot. Eng.*, 2018, **44**, 42–59.

4 K. Bhowmick, S. Roy, M. Mukherjee, G. C. Sahoo, S. Majumdar and P. Mondal, *Mater. Today Proc.*, 2021, **47**, 1496–1499.

5 A. H. Sulaymon, A. O. Sharif and T. K. Al-Shalchi, *J. Chem. Technol. Biotechnol.*, 2011, **86**, 651–657.

6 J. O. Esalah, M. E. Weber and J. H. Vera, *Can. J. Chem. Eng.*, 2000, **78**, 948–954.

7 C. A. Cimá-Mukul, Y. Abdellaoui, M. Abatal, J. Vargas, A. A. Santiago and J. A. Barrón-Zambrano, *Bioinorg. Chem. Appl.*, 2019, **2019**, 1–13.

8 Y. Abdellaoui, M. T. Olguin, M. Abatal, A. Bassam and G. Giácoman-Vallejo, *Desalin. Water Treat.*, 2019, **150**, 157–165.

9 E. Ablouh, A. Essaghraoui, N. Eladlani, M. Rhazi and M. Taourirte, *Water Environ. Res.*, 2019, **91**, 239–249.

10 N. Eladlani, E. M. Dahmane, E. Ablouh, A. Ouahrouch, M. Rhazi, M. Taourirte and M. Neffa, *J. Water Chem. Technol.*, 2019, **41**, 175–181.

11 E. Ablouh, Z. Hanani, N. Eladlani, M. Rhazi and M. Taourirte, *Sustainable Environ. Res.*, 2019, **29**, 5.

12 C. S. C. Chiew, H. K. Yeoh, P. Pasbakhsh, K. Krishnaiah, P. E. Poh, B. T. Tey and E. S. Chan, *Appl. Clay Sci.*, 2016, **119**, 301–310.

13 T. Chen, Z. Zhou, R. Han, R. Meng, H. Wang and W. Lu, *Chemosphere*, 2015, **134**, 286–293.

14 H. Abou Oualid, Y. Abdellaoui, M. Laabd, M. El Ouardi, Y. Brahmi, M. Iazza and J. Abou Oualid, *ACS Omega*, 2020, **5**, 22192–22207.

15 A. Jusoh, L. Su Shiung, N. Ali and M. J. M. M. Noor, *Desalination*, 2007, **206**, 9–16.

16 Y. Achour, L. Bahsis, E.-H. Ablouh, H. Yazid, M. R. Laamari and M. El Haddad, *Surf. Interfaces*, 2021, **23**, 100977.

17 Y. Abdellaoui, H. Abou Oualid, A. Hsini, B. El Ibrahimi, M. Laabd, M. El Ouardi, G. Giácoman-Vallejos and P. Gamero-Melo, *Chem. Eng. J.*, 2021, **404**, 126600.

18 Y. Abdellaoui, P. Gamero-Melo, L. Díaz-Jiménez, C. Ponce-Caballero and G. Giácoman-Vallejos, *Bull. Environ. Contam. Toxicol.*, 2020, **105**, 934–940.

19 Y. Abdellaoui, M. T. Olguín, M. Abatal, B. Ali, S. E. Díaz Méndez and A. A. Santiago, *Superlattices Microstruct.*, 2019, **127**, 165–175.

20 R. El Kaim Billah, Y. Abdellaoui, Z. Anfar, G. Giácoman-Vallejos, M. Agunaou and A. Soufiane, *Water, Air, Soil Pollut.*, 2020, **163**, 1–14.

21 S. Chaouf, S. El Barkany, I. Jilal, Y. El Ouardi, M. Abousalama, M. Loutou, A. El-Houssaine, H. El-Ouarghi, A. El Idrissi and H. Amhamdi, *J. Water Proc. Eng.*, 2019, **31**, 100807.

22 I. Kassem, E.-H. Ablouh, F.-Z. El Bouchtaoui, Z. Kassab, M. Khouloud, H. Sehaqui, H. Ghalfi, J. Alami and M. El Achaby, *Int. J. Biol. Macromol.*, 2021, **189**, 1029–1042.

23 S. Chaouf, S. El Barkany, H. Amhamdi, I. Jilal, Y. El Ouardi, M. Abou-salama, M. Loutou, A. El-Houssaine, H. El Ouarghi and A. El Idrissi, *Mater. Today Proc.*, 2020, **31**, S175–S182.

24 I. Jilal, S. El-Barkany, Z. Bahari, O. Sundman, A. El-Idrissi, M. Abou-Salama, M. Loutou, E. Ablouh and H. Amhamdi, *Mater. Today Proc.*, 2019, **13**, 909–919.

25 P. Liu, H. Sehaqui, P. Tingaut, A. Wichser, K. Oksman and A. P. Mathew, *Cellulose*, 2014, **21**, 449–461.

26 A. Mautner, H. A. Maples, H. Sehaqui, T. Zimmermann, U. Perez De Larraya, A. P. Mathew, C. Y. Lai, K. Li and A. Bismarck, *Environ. Sci.: Water Res. Technol.*, 2016, **2**, 117–124.

27 Z. Li, Y. Gong, D. Zhao, Z. Dang and Z. Lin, *Chemosphere*, 2021, **263**, 128038.

28 S. Chaouf, S. El Barkany, H. Amhamdi, I. Jilal, Y. El Ouardi, M. Abou-salama, M. Loutou, A. El-Houssaine, H. El Ouarghi and A. El Idrissi, *Mater. Today Proc.*, 2020, **31**, S175–S182.

29 M. Hadid, H. Noukrati, H. Ben youcef, A. Barroug and H. Sehaqui, *Cellulose*, 2021, **28**, 7893–7908.

30 J. Lehtonen, J. Hassinen, A. A. Kumar, L.-S. Johansson, R. Mäenpää, N. Pahimanolis, T. Pradeep, O. Ikkala and O. J. Rojas, *Cellulose*, 2020, **27**, 10719–10732.

31 M. El Achaby, Z. Kassab, A. Barakat and A. Aboulkas, *Ind. Crops Prod.*, 2018, **112**, 499–510.

32 D. Hammiche, A. Boukerrou, Y. Grohens, N. Guermazi and F. E. Arrakhiz, *J. Polym. Res.*, 2020, **27**, 308.

33 B. G. Fiss, L. Hatherly, R. S. Stein, T. Friščić and A. Moores, *ACS Sustainable Chem. Eng.*, 2019, **7**, 7951–7959.

34 E.-H. Ablouh, F. Brouillette, M. Taourirte, H. Sehaqui, M. El Achaby and A. Belfkira, *RSC Adv.*, 2021, **11**, 24206–24216.

35 H. El Omari, E. Ablouh, F. Brouillette, M. Taourirte and A. Belfkira, *Cellulose*, 2019, **26**, 9295–9309.

36 F. Kallel, F. Bettaieb, R. Khiari, A. García and J. Bras, *Ind. Crops Prod.*, 2016, **87**, 287–296.

37 Z. Kassab, I. Kassem, H. Hannache, R. Bouhfid, A. E. K. Qaiss and M. El Achaby, *Cellulose*, 2020, **27**, 4287–4303.

38 Z. Marrakchi, R. Khiari, H. Oueslati, E. Mauret and F. Mhenni, *Ind. Crops Prod.*, 2011, **34**, 1572–1582.

39 M. El Achaby, Z. Kassab, A. Barakat and A. Aboulkas, *Ind. Crops Prod.*, 2018, **112**, 499–510.

40 H. S. Barud, C. A. Ribeiro, M. S. Crespi, M. A. U. Martines, J. Dexpert-Ghys, R. F. C. Marques, Y. Messaddeq and S. J. L. Ribeiro, *J. Therm. Anal. Calorim.*, 2007, **87**, 815–818.

41 Z. Zhao, S. Hayashi, W. Xu, Z. Wu, S. Tanaka, S. Sun, M. Zhang, K. Kanayama and K. Umemura, *Polymer*, 2018, **10**, 1251.

42 F. Rol, N. Belgacem, V. Meyer, M. Petit-Conil and J. Bras, *Cellulose*, 2019, **26**, 5635–5651.

43 M. Ghanadpour, F. Carosio, P. T. Larsson and L. Wågberg, *Biomacromolecules*, 2015, **16**, 3399–3410.

44 B. Kayranli, *Alex. Eng. J.*, 2022, **61**, 443–457.

45 I. Ayouch, I. Kassem, Z. Kassab, I. Barrak, A. Barhoun, J. Jacquemin, K. Draoui and M. El Achaby, *Surf. Interfaces*, 2021, **24**, 101124.

46 E. Mahmoudi, S. Azizkhani, A. W. Mohammad, L. Y. Ng, A. Benamor, W. L. Ang and M. Ba-Abbad, *J. Environ. Sci.*, 2020, **98**, 151–160.

47 F. E. Okieimen, C. E. Sogbaike and J. E. Ebhoaye, *Sep. Purif. Technol.*, 2005, **44**, 85–89.

48 X. Yu, S. Tong, M. Ge, L. Wu, J. Zuo, C. Cao and W. Song, *J. Environ. Sci.*, 2013, **25**, 933–943.